CMS Physics Analysis Summary

Contact: cms-pag-conveners-susy@cern.ch 2016/08/04

Search for electroweak SUSY production in multilepton final states in 12.9 fb^{-1} of pp collision data at $\sqrt{s} = 13$ TeV

The CMS Collaboration

Abstract

Searches for the direct electroweak production of supersymmetric charginos and neutralinos are presented in signatures with two light leptons of the same charge and with three or more leptons including up to two hadronically decaying taus. Results are based on a sample of proton-proton collision data collected at a center-of-mass energy $\sqrt{s} = 13$ TeV with the CMS detector in 2016, corresponding to an integrated luminosity of 12.9 fb^{-1}. The observed event rates are in agreement with expectations from the standard model. These results probe charginos and neutralinos with masses up to 400-1000 GeV depending on the assumed model parameters.

1 Introduction

Searches for new physics in the context of supersymmetry (SUSY) [1–9] constitute a major part of the CERN LHC physics programme. While no evidence of such new particles has been found with the samples of proton-proton (pp) collision data collected at $\sqrt{s} = 7$ and 8 TeV, stringent constraints were put on the masses of the colored superpartners (squarks and gluinos) ranging from several hundreds of GeV to about 1.5 TeV, depending on the assumptions entering the models for the interpretation of the results [10]. On the other hand the cross sections associated with electroweak production of SUSY particles are predicted to be far lower than those for strong production. This directly translates in significantly lower exclusion limits on the masses of of sparticles exclusively produced via the electroweak interaction, ranging from about 100 GeV to 700 GeV [11, 12].

In 2015, an increase in the LHC center-of-mass energy to 13 TeV led to a significant rise in the anticipated production cross section for particles with masses of order 1 TeV. As a consequence of this, the reach of searches for strongly coupling new particles already surpassed the results of the previous LHC run with the 2.3 fb^{-1} of data collected in 2015, allowing for the probing of gluinos with masses up to 1.7 TeV [13–16]. As the increase in production cross section of gauginos in the mass range from 200 to 600 GeV is only a factor 2 to 4, the first searches for new particles produced via the electroweak interaction at $\sqrt{s} = 13$ TeV are carried out with the larger sample of 12.9 fb^{-1} of pp collision data, recorded with the CMS detector at the LHC in the first half of 2016.

In this document, we describe searches inspired by signatures characteristic to the direct production of charginos $\widetilde{\chi}^{\pm}$ and neutralinos $\widetilde{\chi}^{0}$, which are the mass eigenstates arising from the SUSY partners of the electroweak gauge and Higgs bosons. Depending on the SUSY mass spectrum, the charginos and neutralinos might prefer to decay to leptons via intermediate sleptons or sneutrinos, the SUSY partners of leptons and neutrinos, as shown in Figs. 1a and 1b. The admixture of gauge eigenstates making up the electroweakinos and charginos, and their masses, will determine whether their decays through sleptons and sneutrinos lead to all three lepton flavors with equal probability (flavor-democratic model), or if they prefer to decay to τ leptons. In the first case, the decays through sleptons as in Fig. 1a and sneutrinos as in Fig. 1b could happen with equal probability, hence leading to the trilepton final state only in 50% of events. In the second case, only the chargino decays might be τ-enhanced (τ-enriched model), or both the charginos and neutralinos might have a preference of decaying to τ's (τ-dominated model). In these scenarios sneutrinos are considered to be heavy and decoupled and do not participate in the cascade decays of gauginos. Hence the fraction of trilepton events grows to 100% for these scenarios. Alternatively, in the absence of low-mass intermediate particles, $\widetilde{\chi}^{\pm}$ and $\widetilde{\chi}^{0}$ can undergo a direct decay to the lightest SUSY particle (LSP) via the emission of W, Z, or Higgs bosons (see Fig. 1c, 1d and 1e), which results in final states with at least two isolated leptons in a fraction of the events. In any case, we assume SUSY scenarios in which R-parity is conserved [9], leading to a stable LSP which escapes detection and manifests itself as missing transverse momentum, $E_{\mathrm{T}}^{\mathrm{miss}}$. Therefore, we carry out the searches for the EWK production of SUSY particles in final states with two light leptons (e or μ) of the same charge (henceforth often referred to as same-sign), and final states with three or more leptons, including up to two hadronically decaying τ's (τ_{h}), all of these accompanied by $E_{\mathrm{T}}^{\mathrm{miss}}$.

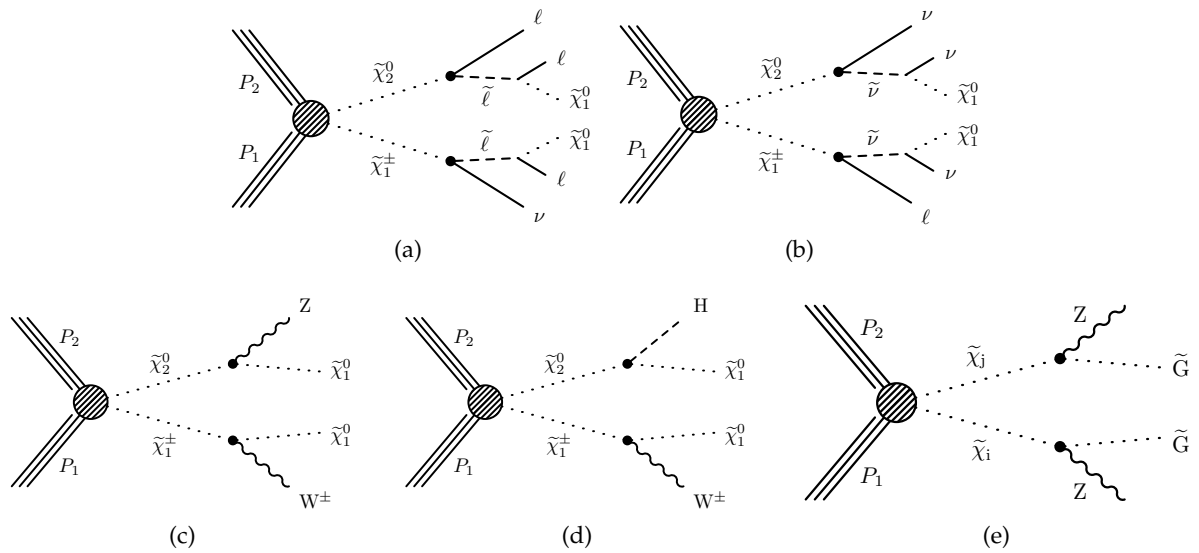

Figure 1: Chargino-neutralino pair production with decays mediated by (a) sleptons and (b) sneutrinos and leading to leptonic final states. Chargino-neutralino pair production decaying directly to an LSP via a W and (c) a Z boson or (d) a Higgs boson. (e) Gaugino pair production decaying to a gravitino LSP via a Z boson.

2 Event selection and Monte Carlo simulation

A detailed description of the CMS detector, together with a definition of the coordinate system and the relevant kinematic variables, can be found in Ref. [17].

The analyzed events are recorded with several sets of online event selection algorithms called triggers, requiring the presence of either one e or μ, or two leptons (e, μ or τ). The searches with at least two e or μ in the final state rely on dilepton triggers with very loose isolation requirements and $p_{\mathrm{T}} > 17\ (23)\,\mathrm{GeV}$ for the leading and $p_{\mathrm{T}} > 8\ (12)\,\mathrm{GeV}$ for the subleading muon (electron). For the final state with two τ_{h} and one e or μ a combination of several trigger algorithms is utilized: single lepton triggers requiring an isolated μ (e) with $p_{\mathrm{T}} > 22\ (27)\,\mathrm{GeV}$, and triggers including τ_{h} selection, demanding events with one μ (e) with $p_{\mathrm{T}} > 19\ (22)\,\mathrm{GeV}$ and $|\eta| < 2.1$ and a τ_{h} with $p_{\mathrm{T}} > 20\,\mathrm{GeV}$.

Typical trigger efficiencies for leptons satisfying the offline selection criteria applied in this search as described below, are 92% (98%) per muon (electron), and 96% per τ_{h}. In final states with three or more leptons, the total trigger efficiency is close to 100% due to a higher probability of a positive trigger decision induced by the presence of an extra lepton.

In the offline analysis, the information from all sub-detectors is combined by the CMS particle-flow (PF) algorithm [18, 19] in order to reconstruct and identify individual particles and to provide a global interpretation of the event. The particles are classified into charged hadrons, neutral hadrons, photons, muons and electrons.

PF candidates are clustered into jets using the anti-k_{T} algorithm with a distance parameter $\Delta R = \sqrt{\Delta\eta^2 + \Delta\phi^2}$ of 0.4, as implemented in the FASTJET package [20, 21]. Jets are required to satisfy quality requirements [22] to remove those consistent with anomalous energy deposits. Charged hadrons are not considered if they do not originate from the selected primary vertex, that is, the collision vertex for which the summed p_{T}^2 of the associated tracks is the largest. After the estimated contribution from additional pp interactions in the same or adjacent bunch crossings (pileup) is subtracted, jet energies are corrected for residual non-uniformity and non-

linearity of the detector response using simulation and data. Only jets with $p_T > 25\,\text{GeV}$, $|\eta| < 2.4$ and separated from any lepton candidate by $\Delta R > 0.4$ are retained.

To identify jets originating from b quarks, the combined secondary vertex algorithm CSVv2 [23] is used. Jets with $p_T > 25\,\text{GeV}$ and $|\eta| < 2.4$ are considered as b-tagged if they satisfy the requirements of the medium working point of the algorithm. These requirements result in an efficiency of approximately 70% for tagging a b-quark jet, and a mistagging rate of less than 1% for light-quark and gluon jets in $\mathrm{t\bar{t}}$ events. Simulated events are corrected for differences in the performance of the algorithm between data and simulation. Events with at least one identified b jet are vetoed in the analysis to reduce the $\mathrm{t\bar{t}}$ background.

The E_T^{miss} is calculated as the negative vector sum of the transverse momenta of all reconstructed particles, after jets have been clustered and jet energy corrections have been applied [24].

Muon candidates are reconstructed combining the information from both the silicon tracker and the muon spectrometer in a global fit [25]. An identification selection is performed using the quality of the geometrical matching between the tracker and the muon system measurements. Only muons within the muon system acceptance $|\eta| < 2.4$ and a minimum p_T of 10 GeV are considered.

Electrons are reconstructed using tracking and electromagnetic calorimeter information by combining ECAL superclusters and Gaussian sum filter (GSF) tracks [26]. We require electrons to have $|\eta| < 2.5$, to ensure that they are within the tracking volume, and a minimum p_T of 10 GeV. The electron identification is performed using a multivariate discriminant built from shower-shape variables and track quality variables. Further requirements are applied to reject electrons from photon conversions, by rejecting candidates with missing hits in the innermost layers of the tracking system or matched to a secondary conversion vertex candidate [26].

Lepton candidates are required to be consistent with originating from the primary vertex. The transverse d_0 (longitudinal d_z) impact parameter of the leptons must not exceed 0.5 (1.0) mm with respect to this vertex, and these leptons must satisfy a requirement on the impact parameter significance $\text{SIP}_{3D} = |d_{3D}|/\sigma(d_{3D}) < 8$, where d_{3D} is the three-dimensional impact parameter with respect to the vertex and $\sigma(d_{3D})$ is its uncertainty, as estimated from the track fit.

To distinguish between leptons originating from decays of heavy particles such as W and Z bosons or SUSY particles ("prompt" leptons) and those produced in hadron decays or in photon conversions as well as hadrons misidentified as leptons ("non-prompt" leptons), information about the local isolation of the leptons is used. The miniisolation variable (I_{mini}) [16, 27] is computed as the ratio between the scalar p_T sum of charged hadrons, neutral hadrons, and photons within a cone around the lepton candidate direction at the vertex, whose size depends on the transverse momentum of the lepton candidate ($p_T(\ell)$), and $p_T(\ell)$ itself. The cone radius ΔR depends on $p_T(\ell)$ as:

$$\Delta R\left(p_T(\ell)\right) = \frac{10\,\text{GeV}}{\min\left[\max\left(p_T(\ell), 50\,\text{GeV}\right), 200\,\text{GeV}\right]}. \tag{1}$$

The varying isolation cone definition takes into account the increased collimation of the decay products of a hadron as its p_T increases, and it reduces the inefficiency from accidental overlap between the lepton and other objects in an event. Loosely isolated leptons are required to have $I_{\text{mini}} < 0.4$. Electrons and muons that pass all the aforementioned requirements are referred to as *loose* in this analysis.

To retain the highest possible efficiency to identify prompt leptons while rejecting non-prompt

leptons from background processes, advanced identification criteria developed in Ref. [28] are employed. In particular, we use the following variables as an input to a multivariate discriminator based on a boosted decision tree (BDT) [29]:

- vertexing variables: d_0, d_z, SIP_{3D};
- miniisolation I_{mini};
- variables related to the jet closest to the lepton, such as the ratio between the p_{T} of the lepton and the p_{T} of the jet ($p_{\mathrm{T}}^{\mathrm{ratio}}$), the CSV b-tagging discriminator value of the jet, the number of charged particles in the jet, and the $p_{\mathrm{T}}^{\mathrm{rel}}$ variable:

$$p_{\mathrm{T}}^{\mathrm{rel}} = \frac{|(\vec{p}(\mathrm{jet}) - \vec{p}(\ell)) \times \vec{p}(\ell)|}{|\vec{p}(\mathrm{jet}) - \vec{p}(\ell)|}; \quad (2)$$

- variables used in the identification of the electron and muon candidates: the muon segment compatibility, and the electron identification multivariate discriminant.

Electrons and muons satisfying a requirement on the discriminator value in addition to passing the loose lepton selection are defined as *tight* in the analysis. In particular a medium requirement on the multivariate discriminant is applied in the three lepton search regions, while the two same-sign lepton search regions use a very tight requirement on this discriminator.

The reconstruction of τ_{h}'s used the the hadron-plus-strips algorithm [30]. τ_{h} candidates are required to pass the "decay mode finding" discriminator, either being reconstructed in 1- or 3-prong decay modes with or without additional π^0 particles. In addition, they have to fulfill $p_{\mathrm{T}} > 20\,\mathrm{GeV}$, $|\eta| < 2.3$, and isolation requirements in a $\Delta R = 0.5$ cone. The typical τ_{h} identification efficiency of these selection requirements is 50% while the jet misidentification rate is well below 0.1% [31].

Monte Carlo (MC) simulated samples, which includes pileup, are used to estimate the background from standard model (SM) processes with prompt leptons (see Section 4) and to calculate the selection efficiency for various new-physics scenarios. The SM background samples are produced with the MADGRAPH5_AMC@NLO v2.2.2 generator [32] at leading order (LO) or next-to-leading order (NLO) accuracy in perturbative quantum chromodynamics, with the exception of diboson samples which are produced with the POWHEG v2 [33, 34] generator. The NNPDF3.0LO [35] parton distribution functions (PDFs) are used for the simulated samples generated at LO and the NNPDF3.0NLO [35] PDFs for the samples generated at NLO. Parton showering and hadronization are described using the PYTHIA 8.205 generator [36] with the CUETP8M1 tune [37, 38]. The CMS detector response for the background samples is modeled with the GEANT4 package [39].

Signal samples are generated with MADGRAPH5_AMC@NLO at LO precision, including up to two additional partons in the matrix element calculations; Parton showering and hadronization as well as decays of SUSY particles are simulated with PYTHIA 8.205 while the detector simulation is performed with the CMS fast simulation package [40].

3 Search strategy

This search is designed to cover a broad range of possible new physics scenarios which manifest themselves in multilepton or same-sign dilepton signatures with little to no hadronic activity. An additional characteristic of the signals under consideration is the presence of particles in final states that evade detection, yielding a sizable $E_{\mathrm{T}}^{\mathrm{miss}}$. The specific strategy of the analysis is guided by R-parity conserving SUSY models in which new particles are produced through

the electroweak interaction, potentially leading to a vast variety of signatures. In the context of the simplified models of new-particle production [41, 42] shown in Fig. 1, we might get final states with three leptons of different flavor and charge combinations, both resonant (from W and Z boson decay) and non-resonant. The signature with two leptons of the same charge can arise in case one of the leptons is too soft to be detected, as is expected to occur in models with a compressed mass spectrum.

With this in mind, the analysis is subdivided into several categories defined by the number of leptons in the event, their flavor and charge. Each of these categories is further subdivided into bins defined by the kinematic variables such as the invariant mass of the two leptons forming an opposite-sign dilepton pair (if any) ($M_{\ell\ell}$), the transverse mass of the third lepton and $E_{\mathrm{T}}^{\mathrm{miss}}$ system (M_{T}), the two-lepton transverse mass (M_{T2}) [43, 44], and $E_{\mathrm{T}}^{\mathrm{miss}}$. These variables are chosen to either suppress background contributions arising from standard model processes or to enhance the sensitivity to possible mass hierarchies of new particles.

3.1 Search regions in the three-lepton final state

Events are selected on the condition that they contain exactly three leptons passing the identification criteria, among which are at maximum two τ_{h}'s. The leading electron (muon) must satisfy $p_{\mathrm{T}} > 25\ (20)$ GeV, while the subleading electron (muon) must satisfy $p_{\mathrm{T}} > 15\ (10)$ GeV, criteria originating from the p_{T} thresholds of the dilepton triggers used in the analysis. Moreover, in an event with a leading muon, if the other leptons are electrons or taus, the leading muon is required to have $p_{\mathrm{T}} > 25$ GeV. For events with one e or μ and two τ_{h}, all leptons are additionally constrained to have $|\eta| < 2.1$, and an electron (muon) should have $p_{\mathrm{T}} > 30\ (25)$ GeV. To reduce the contribution from the processes with low-mass resonances, events are vetoed if they contain an opposite-sign same-flavor (OSSF) pair with an invariant mass below 12 GeV. Additionally in events containing an OSSF pair of two e or μ, the invariant mass of all three leptons is required not to be consistent with the mass of a Z boson ($|M_{3\ell} - M_{\mathrm{Z}}| > 15$ GeV) in order to suppress contributions from asymmetric photon conversions.

A first categorization of events is done according to the flavor of the identified leptons, and the number of opposite-sign dilepton pairs:

A: three e or μ with two of the leptons forming an OSSF pair

B: three e or μ but no OSSF pair

C: two e or μ forming and OSSF pair, and one τ_{h}

D: an opposite-sign eμ pair and one τ_{h}

E: a same-sign pair of e or μ and one τ_{h}

F: one e or μ and two τ_{h}

These search regions are then further subdivided according to their kinematic properties. The most prominent events are those of category A - three e or μ with two of the leptons forming an OSSF pair. The first variable used for the search region binning is the invariant mass of the dilepton pair, $M_{\ell\ell}$. A leptonically decaying Z-boson leads to a pair of leptons with an invariant mass close to the Z-boson mass. This makes $M_{\ell\ell}$ a powerful discrimination tool for separating events with and without a Z-boson involved in the decay chain and it motivates the separation of the events under consideration into three $M_{\ell\ell}$ bins. Two of the $M_{\ell\ell}$ bins are defined to be above and below the Z mass, while the third one is defined as the Z mass window, and it is

expected to contain the bulk of the standard model background events. When an event contains an OSSF pair and a third lepton of a different flavor there is no ambiguity as to which leptons are used to compute $M_{\ell\ell}$. In the case of three leptons having the same flavor, the OSSF pair with the invariant mass closest to the mass of the Z-boson is used. The transverse mass M_{T} of the third lepton in the event is computed with respect to $E_{\mathrm{T}}^{\mathrm{miss}}$. Both variables, M_{T} and $E_{\mathrm{T}}^{\mathrm{miss}}$, are used to further categorize the events with most of the standard model background expected in low M_{T} and $E_{\mathrm{T}}^{\mathrm{miss}}$ bins. The search regions for events of category A are summarized in Table 1.

In the rarer case of three e or μ, none of them forming an OSSF pair, two bins each for $M_{\ell\ell}$ and M_{T} are used. The low M_{T} bins are then further subdivided into two $E_{\mathrm{T}}^{\mathrm{miss}}$ bins. These search regions are listed in Table 2. As these events mostly originate from standard model processes leading to leptonically decaying τ, the $M_{\ell\ell}$ is calculated from the opposite sign (OS) dilepton pair whose invariant mass is closest to the mean dilepton mass determined from $Z \to \tau\tau$ simulation, which is 50 GeV. If no OS pair is found, the event is automatically assigned to the lowest $M_{\ell\ell}$ bin, and the M_{T} is taken to be the minimal M_{T} out of the three leptons in the event.

Thirdly, the category of two e or μ forming an OSSF pair, conjoined by a τ_{h}, uses the same three $M_{\ell\ell}$ bins as in category A, again with the goal to separate off-Z and on-Z regions. For all events with a τ_{h}, M_{T2} replaces M_{T} for the further subdivision of the bins, as M_{T2} is found to be a more powerful discriminator with respect to the $\mathrm{t\bar{t}}$ background. The M_{T2} variable is computed with a pair of leptons which is most likely to come from leptonic decays of W bosons in the $\mathrm{t\bar{t}}$ process. Since a probability to misidentify a τ_{h} is much larger than the one to misidentify an electron or a muon, M_{T2} is computed with a pair of light leptons in this category. The lower M_{T2} bin contains the vast majority of the SM background events among which $\mathrm{t\bar{t}}$ is dominant. For the search regions containing a Z candidate, the splitting in terms of M_{T2} is not performed. The complete set of signal regions for events in category C is given in Table 3.

For events with a τ_{h} and two light leptons that do not form an OSSF pair (i.e. $\mathrm{e^{\pm}e^{\pm}}$, $\mu^{\pm}\mu^{\pm}$, $\mu^{\pm}\mathrm{e}^{\mp}$, $\mu^{\pm}\mathrm{e}^{\pm}$), the OS pair, if present, with the invariant mass closest to the corresponding dilepton mass expected from a $\mathrm{Z} \to \tau\tau$ decay (50 GeV for eμ and 60 GeV for eτ_{h} or $\mu\tau_{\mathrm{h}}$) is used for the event categorization. If no OS pair is present, the event is again sent to the lowest $M_{\ell\ell}$ bin. In this case, further categorization is done depending on whether the e or μ form an OS or SS pair, and the final search region binning is shown in Table 4 and 5. The M_{T2} variable is computed with a pair of the opposite-sign light leptons if it is present in an event, otherwise with a leading in p_{T} light lepton and a τ_{h}.

The last category accommodates events with two τ_{h}'s and an e or μ, for which the binning is shown in Table 6. The M_{T2} variable is computed with a light lepton and a leading in p_{T} τ_{h}.

Table 1: Search regions for events with three e or μ that form at least one OSSF pair.

M_{T} (GeV)	$E_{\mathrm{T}}^{\mathrm{miss}}$ (GeV)	$M_{\ell\ell} < 75\,\mathrm{GeV}$	$75\,\mathrm{GeV} \leq M_{\ell\ell} < 105\,\mathrm{GeV}$	$M_{\ell\ell} \geq 105\,\mathrm{GeV}$
$0-120$	$50-100$	SR A01	SR A13	SR A25
	$100-150$	SR A02	SR A14	SR A26
	$150-200$	SR A03	SR A15	SR A27
	>200	SR A04	SR A16	SR A28
$120-160$	$50-100$	SR A05	SR A17	SR A29
	$100-150$	SR A06	SR A18	SR A30
	$150-200$	SR A07	SR A19	SR A31
	>200	SR A08	SR A20	SR A32
>160	$50-100$	SR A09	SR A21	SR A33
	$100-150$	SR A10	SR A22	SR A34
	$150-200$	SR A11	SR A23	SR A35
	>200	SR A12	SR A24	SR A36

Table 2: Search regions for events with three e or μ that do not form an OSSF pair.

M_{T} (GeV)	$E_{\mathrm{T}}^{\mathrm{miss}}$ (GeV)	$M_{\ell\ell} < 100\,\mathrm{GeV}$	$M_{\ell\ell} \geq 100\,\mathrm{GeV}$
$0-120$	$50-100$	SR B01	SR B04
	>100	SR B02	SR B05
>120	>50	SR B03	SR B06

Table 3: Search region definition for events with 2 e or μ forming an OSSF pair and one τ_{h}. Regions where there is a Z candidate are not split in M_{T2} categories.

$M_{\mathrm{T2}}(\ell_1,\ell_2)$ (GeV)	$E_{\mathrm{T}}^{\mathrm{miss}}$ (GeV)	$M_{\ell\ell} < 75\,\mathrm{GeV}$	$75\,\mathrm{GeV} \leq M_{\ell\ell} < 105\,\mathrm{GeV}$	$M_{\ell\ell} \geq 105\,\mathrm{GeV}$
<100	$50-100$	SR C01	SR C05	SR C09
	$100-150$	SR C02	SR C06	SR C10
	$150-200$	SR C03	SR C07	SR C11
	>200	SR C04	SR C08	SR C12
≥ 100	$50-200$	SR C13	SR C05 – SR C07	SR C13
	>200	SR C14	SR C08	SR C14

Table 4: Search region definition for events with one e and one μ of opposite charge and one τ_{h}.

$M_{\mathrm{T2}}(\ell_1,\ell_2)$ (GeV)	$E_{\mathrm{T}}^{\mathrm{miss}}$ (GeV)	$M_{\ell\ell} < 60\,\mathrm{GeV}$	$60 \leq M_{\ell\ell} < 100\,\mathrm{GeV}$	$M_{\ell\ell} \geq 100\,\mathrm{GeV}$
<100	$50-100$	SR D01	SR D05	SR D09
	$100-150$	SR D02	SR D06	SR D10
	$150-200$	SR D03	SR D07	SR D11
	>200	SR D04	SR D08	SR D12
≥ 100	$50-200$	SR D13		
	>200	SR D14		

Table 5: Search region definition for events with 2 e or μ of the same charge and one τ_{h}.

$M_{\mathrm{T2}}(\ell_1,\tau)$ (GeV)	$E_{\mathrm{T}}^{\mathrm{miss}}$ (GeV)	$M_{\ell\ell} < 60\,\mathrm{GeV}$	$60 \leq M_{\ell\ell} < 100\,\mathrm{GeV}$	$M_{\ell\ell} \geq 100\,\mathrm{GeV}$
<100	$50-100$	SR E01	SR E05	SR E09
	$100-150$	SR E02	SR E06	
	$150-200$	SR E03	SR E07	
	>200	SR E04	SR E08	
≥ 100	>50	SR E10		

Table 6: Search region definition for events with one electron or muon and 2 τ_{h}.

$M_{\mathrm{T2}}(\ell,\tau_1)$ (GeV)	$E_{\mathrm{T}}^{\mathrm{miss}}$ (GeV)	$M_{\ell\ell} < 100\,\mathrm{GeV}$	$M_{\ell\ell} \geq 100\,\mathrm{GeV}$
<100	$50-100$	SR F01	SR F04
	$100-150$	SR F02	SR F05
	>150	SR F03	SR F06
≥ 100	$50-200$	SR F07	
	>200	SR F08	

3.2 Search regions in the four-lepton final state

Events with four leptons in the final state have markedly lower standard model backgrounds compared to the trilepton category, and are therefore grouped into fewer search regions. The search regions are formed according to the number of OSSF pairs and the number of τ_{h}'s in the event, and are defined as:

G: at least four e or μ among which there are two OSSF pairs not sharing a lepton

H: at least four e or μ among which there are less than two OSSF pairs which don't share a lepton

I: at least four leptons among which there are one or more τ_{h}'s.

The data are further subdivided in intervals of $E_{\mathrm{T}}^{\mathrm{miss}}$ with the goal to more efficiently discriminate between signal and background. The search region definitions and their notations are summarized in Table 7.

Table 7: Search region definition for events with four or more leptons.

$E_{\mathrm{T}}^{\mathrm{miss}}$ (GeV)	$0\tau_{\mathrm{h}}$		$\geq 1\tau_{\mathrm{h}}$
	nOSSF ≥ 2	nOSSF ≤ 1	nOSSF ≥ 0
$0-30$	SR G01	SR H01	SR I01
$30-50$	SR G02	SR H02	SR I02
$50-100$	SR G03	SR H03	SR I03
>100	SR G04	SR H04	SR I04

3.3 Search in the same-sign two-lepton final state

The three-lepton analysis discussed above is not sensitive to the chargino-neutralino pair production processes depicted in Fig. 1 in case one of the leptons remains unidentified, non-isolated, or in any way outside of the acceptance of the analysis. In compressed SUSY scenarios one of the leptons from the cascade decays of a neutralino can however be very soft, such that it would not be included in the analysis, and the event would fail the three lepton event selection criteria. To recover sensitivity to these scenarios, we form search regions where we require exactly two light leptons (ee, eμ, or $\mu\mu$), which we additionally oblige to have the same charge, as opposite-charge lepton pairs are copiously produced by several standard model processes.

The leptons must satisfy $p_{\mathrm{T}} > 25\ (20)$ GeV for the leading and $p_{\mathrm{T}} > 15\ (10)$ GeV for the trailing electron (muon). To suppress the WZ background, events are vetoed if they contain an OSSF pair formed from loose e's or μ's in a 15 GeV window around the Z boson mass.

To further increase the sensitivity towards more compressed scenarios, the phase space is divided into events with and without an ISR-jet ($p_{\mathrm{T}} > 40$ GeV). Subsequent binning is done using $E_{\mathrm{T}}^{\mathrm{miss}}$, the minimal M_{T} computed from one of the leptons and the $E_{\mathrm{T}}^{\mathrm{miss}}$, and the transverse momentum of the dilepton system $p_{\mathrm{T}}^{\ell\ell}$. The different search regions for this category of events are summarized in Table 8.

Table 8: Search regions for events with two same-sign light flavor leptons.

N_{jets}	M_{T} (GeV)	$p_{\mathrm{T}}^{\ell\ell}$ (GeV)	$E_{\mathrm{T}}^{\mathrm{miss}} < 100$ GeV	100 GeV $\leq E_{\mathrm{T}}^{\mathrm{miss}} < 150$ GeV	$E_{\mathrm{T}}^{\mathrm{miss}} \geq 150$ GeV
0	<100	<50	SS 01	SS 02	SS 03
		≥ 50	SS 04	SS 05	SS 06
	≥ 100	<50	SS 07	SS 08	SS 09
		≥ 50			
1	<100	<50	SS 10	SS 11	SS 12
		≥ 50	SS 13	SS 14	SS 15
	≥ 100	<50	SS 16	SS 17	SS 18
		≥ 50			

4 Backgrounds

The standard model backgrounds leading to the final states under consideration can be subdivided into the following categories:

- **WZ production:** In case both W and Z bosons decay leptonically, they produce the same signature as the new physics scenarios targeted by this analysis: three energetic

and isolated leptons and a sizable $E_{\mathrm{T}}^{\mathrm{miss}}$ due to a neutrino from the W boson decay. This is the dominant background by a large margin in the searches with three e or μ forming an OSSF dilepton pair. WZ events also contribute to the same-sign dilepton signature when the Z boson is off-shell, in which case one of the leptons from the Z boson decay might fail the applied selection criteria, or when the Z boson decays to τ leptons yielding a semileptonic final state.

- **Non-prompt e, μ and τ_{h}:** Non-prompt leptons are leptons from heavy-flavor decays, misidentified hadrons, muons from light-mesons that decay in flight, or electrons from unidentified conversions of photons in jets. Depending on the considered lepton multiplicity, this background is dominated by the W + jets (especially in same-sign dilepton regions), $\mathrm{t\bar{t}}$ and DY+jets processes. This category provides the largest background contribution in the trilepton search regions without an OSSF pair, and those with a τ_{h} candidate.
- **External and internal conversions:** These processes contribute to the same-sign dilepton or trilepton final states when a W or a Z boson radiates an initial- or final-state photon and this photon undergoes an asymmetric internal or external conversion in which one of the leptons has very low p_{T}. This soft lepton has a high probability of failing the selection criteria of the analysis, leading to a reconstructed two- (in case of a W boson) or three-lepton (in case of a Z boson) final state. This background mostly contributes to categories with an OSSF pair and to final states with two leptons of the same charge.
- **Rare SM processes with multiple prompt leptons:** Standard model processes that yield a same-sign lepton pair, or three or more leptons include multi-boson production (W, Z, H, or a prompt γ), single boson production in association with a $\mathrm{t\bar{t}}$ pair, and double-parton scattering. Such processes generally have very small production rate and can in some cases be further suppressed by the b-jet veto.
- **Charge misidentification:** A background from charge misidentification arises from events with an OS pair of isolated eμ or ee in which the charge of one of the electrons is misidentified. In most cases, this arises due to severe bremsstrahlung in the tracker material. This is a small background, manifesting itself in the same-sign dilepton category or in the category with a same-sign dilepton pair and a τ_{h}.

The WZ background is normalized to data in a control region adjacent to the same-sign dilepton search region, obtained by inverting the veto on the presence of a third lepton, and requiring an on-Z OSSF pair to be present. Additional requirements applied for events to enter the control region are $M_{\mathrm{T}} < 120\,\mathrm{GeV}$ and $35\,\mathrm{GeV} < E_{\mathrm{T}}^{\mathrm{miss}} < 100\,\mathrm{GeV}$, where upper thresholds correspond to the definition of the search region SR A13 of the trilepton search category. As a consequence of the overlap with search region SR A13, the latter region is not used in the interpretation of the results in terms of new physics models. The uncertainty in the normalization is found to be 9–11%, where the larger values are used to account for the possible signal contamination, and are only applied for the interpretations where this potential contamination is not negligible in the control region.

In order to estimate the convoluted effects from potential mismodeling of the W M_{T} shape in the simulation of the WZ process, which might for instance be induced by a different $E_{\mathrm{T}}^{\mathrm{miss}}$ resolution in data compared to simulation, the M_{T} shape prediction of the simulation is verified in a Wγ and W + jets control sample in data. After drastically reducing the contribution of Wγ events produced by means of final state radiation (FSR) of the photon, by applying a high p_{T} threshold on the photon, the W M_{T} shapes in the Wγ, W + jets and WZ processes were

shown to be the same. The Wγ and W + jets M_{T} shape was thereafter measured in a dedicated control sample in which an energetic well identified and isolated photon with $p_{\mathrm{T}} > 50\,\mathrm{GeV}$ was required, together with a lepton passing the same criteria as those selected in the trilepton search regions, and $E_{\mathrm{T}}^{\mathrm{miss}} > 50\,\mathrm{GeV}$. A minimum separation of $\Delta R > 0.3$ was required between the lepton and the photon to further reduce the FSR contribution. After subtraction of the residual contamination from processes other than Wγ or W + jets, the M_{T} shape measured in this control region was compared to the one predicted by the WZ simulation. The measured shape was found to agree well with the simulated prediction within the statistical uncertainties, and the precision of this comparison is used to derive systematic uncertainties on the high M_{T} bins of the trilepton search.

The background from non-prompt light leptons is estimated by using the "tight-to-loose" ratio method which is described in detail in Refs. [16, 28]. The probability for a loosely defined light lepton to pass the full set of selection criteria is measured in a multi-jet sample in data enriched in non-prompt leptons, called the measurement region. Once measured, this probability is applied in a sample of events which pass the full kinematic selection, but where at least one of the leptons fails the nominal selection but passes the loose requirements, in order to predict the number of events from non-prompt leptons entering each search region. The contribution from non-prompt τ_{h}'s is estimated in a similar way. This time, the "tight-to-loose" ratio is measured in a Z+jets enriched control sample in data, in which a τ_{h} is required to be present in addition to an OSSF pair from a leptonically decaying Z. The residual contribution from prompt leptons in the measurement and application regions is subtracted using MC simulation. It is verified in both MC simulation and low-$E_{\mathrm{T}}^{\mathrm{miss}}$ data control regions, that this method describes the background from the non-prompt leptons entering the different search regions within a systematic uncertainty of 30%.

The modeling of the conversion background is verified in a data control region enriched in both external and internal conversions. The rate of $\mathrm{Z} \to 3\ell$ events is compared with the full prediction derived from the MC simulation and the non-prompt leptons, in an off-Z control region defined by $|M_{\ell\ell} - M_{\mathrm{Z}}| > 15\,\mathrm{GeV}$ and $E_{\mathrm{T}}^{\mathrm{miss}} < 50\,\mathrm{GeV}$. The predicted background yields are found to agree with the simulation within the statistical uncertainties.

The charge misidentification background in the same-sign dilepton channel is estimated by reweighing the events with opposite-sign lepton pairs by the charge misidentification probability. For electrons this probability is obtained from simulated $\mathrm{t\bar{t}}$ events and from an on-Z $\mathrm{e^{\pm}e^{\pm}}$ control region in data, and it lies in the range 10^{-5}–10^{-3} depending on the electron's p_{T} and η. Studies of the simulated events indicate that the muon charge misidentification probability is negligible. In the case of the same-sign dilepton and a τ_{h} final state, the charge misidentification background from WZ and rare standard model processes is taken directly from the simulation and is not presented as a separate category.

5 Systematic uncertainties

The systematic uncertainties on the background estimation and signal acceptance affect both the overall normalization of the yields, and the relative population of the processes in the search regions. A list of systematic uncertainties considered in this analysis is summarized in Table 9.

Experimental uncertainties include uncertainties on the lepton selection efficiency, the trigger efficiency, the jet energy scale and b-tag veto efficiency, and the object selection efficiencies are generally different in data and MC. Lepton identification and trigger efficiencies are computed with the "tag-and-probe" technique [25, 26], respectively with an uncertainty of 3 and 4% per

Table 9: Summary of systematic uncertainties in the event yields in the search regions. The upper group lists uncertainties related to experimental factors for all processes whose yield is estimated from simulation; the middle group lists uncertainties in these yields related to the event simulation process itself. The lower group lists uncertainties for background processes whose yield is estimated from data.

Source	estimated uncertainty (%)
e/μ selection	3
τ_h selection	6
Trigger efficiency	1–4
Jet energy scale	2–10
b tag veto	5
Pileup	1–5
Integrated luminosity	6.2
Theoretical ($t\bar{t}Z$ and $t\bar{t}W$)	15
Theoretical (ZZ)	25
Conversions	20-50
Other backgrounds	50
Monte Carlo statistical precision	1–30
Nonprompt leptons	30–36
Charge misidentification	30
WZ normalization	9–11
WZ shape	10–80

lepton. The τ_h identification efficiency on the other hand, is determined to within an uncertainty of 6% [31].

The total effect of the trigger efficiency and its uncertainty varies between the different search regions, being most important for the same-sign dilepton search, where it is estimated to be 4%. In the three- and four-lepton final states, the trigger efficiency is close to 100% due to the presence of one or two extra leptons in the events, and the corresponding uncertainties on this efficiency are respectively 3 and 1%.

The jet energy scale uncertainty varies between 2 and 8%, depending on p_T and η of the jet. This uncertainty affects other event quantities like the b-tag veto, E_T^{miss}, M_T and M_{T2}, and is computed by shifting the energy of each jet coherently and propagating the variation to all these kinematic variables. Correlation effects due to the migration of events from one search region to another are taken into account. These variations yield estimated uncertainties ranging from 2 to 10%, on the simulated signal and background yields in the different search regions. Similarly, the b-jet veto efficiency is corrected for the differences between data and MC simulation, and an associated uncertainty on this correction is derived. The uncertainty in the modeling of pileup is 1–5%, depending on the search region, and the uncertainty on the integrated luminosity is 6.2% [45].

The uncertainty on the normalization of the WZ background is assessed to be 9–11%. This includes statistical uncertainties on the yields in the control sample used for normalization, and the systematic uncertainty due to the subtraction of all the non-WZ backgrounds. An additional uncertainty on the predicted WZ background yields stems from the modeling of the M_T shape in the simulation of the WZ process. This uncertainty is found to be between 10 and 50%, by comparing the M_T shape in the WZ MC simulation to the one measured in the Wγ control region. The size of this uncertainty increases for higher M_T values and is driven by the statistical uncertainty in Wγ the control sample.

Further uncertainties on backgrounds estimated from simulations arise from the unknown higher-order effects in the theoretical calculations of the cross sections, and from uncertainties in the knowledge of the proton's PDFs. The effect of these kind of theoretical uncertainties is found to be 15% for $t\bar{t}W$ and $t\bar{t}Z$ and 25% for ZZ. Theoretical uncertainties are also considered for the remaining minor backgrounds estimated purely from simulation, in which 20% uncertainty is assigned to processes with a prompt γ modeled with NLO accuracy, and 50% to those modeled with LO accuracy and to the sum of the other rare processes.

Other sources of uncertainties concern the backgrounds which are derived from, or normalized in data control samples. The non-prompt background prediction has an uncertainty of 30% assigned for both light lepton and τ_h cases. This uncertainty arises from the performance of the method in the simulation in various phase space regions, and is derived to describe the observed deviations between the estimated and observed yields.

The uncertainty on the measurement of the charge misidentification background is derived from the difference between the yields of on-Z $e^{\pm}e^{\pm}$ events in data and the simulation. This uncertainty is found to be equal to 30%.

6 Results

The expected and observed yields in the categories used in the analysis yields are summarized in Tables 10-15 for trilepton search regions, in Table 16 for four-lepton ones, and in Table 17 for the same-sign channel. The observed events counts are consistent with the ones expected from the SM processes. The two search regions in the same-sign dilepton search with the most significant discrepancies between the observed data and the predicted background correspond to the selection $N_{\text{jets}} = 1$, $M_{\text{T}} < 100\,\text{GeV}$, $E_{\text{T}}^{\text{miss}} \geq 150\,\text{GeV}$, and differ in the requirement on the transverse momentum of the dilepton system $p_{\text{T}}^{\ell\ell}$. The observed excess of events above the expected SM background corresponds to a local significance of 1.7σ for the region with $p_{\text{T}}^{\ell\ell} < 50\,\text{GeV}$, and of 2.5σ for the region with $p_{\text{T}}^{\ell\ell} \geq 50\,\text{GeV}$.

The comparison between the expected and observed yields are presented in Fig. 2-4 for the trilepton search regions, in Fig. 5 for search regions with at least four leptons, and in Fig. 6 for the same-sign dilepton search regions.

Table 10: Expected and observed yields in events with three e or μ that form one OSSF pair. Uncertainty denotes total uncertainty on the result.

M_{T} (GeV)	$E_{\text{T}}^{\text{miss}}$ (GeV)	$m_{\ell\ell} < 75\,\text{GeV}$		$75 \leq m_{\ell\ell} < 105\,\text{GeV}$		$m_{\ell\ell} \geq 105\,\text{GeV}$	
$0-120$	$50-100$	82 ± 11	94	900 ± 100	933	56 ± 8	40
	$100-150$	20 ± 4	22	170 ± 33	175	14 ± 3	11
	$150-200$	4.4 ± 1.3	4	49 ± 12	48	3.7 ± 1.0	6
	>200	2.3 ± 0.6	2	36 ± 10	35	4.6 ± 1.4	5
$120-160$	$50-100$	8.0 ± 2.2	14	40 ± 16	41	4.7 ± 1.5	4
	$100-150$	2.5 ± 1.0	4	8.0 ± 2.9	7	1.8 ± 0.6	2
	$150-200$	0.7 ± 0.3	0	1.2 ± 0.6	3	0.8 ± 0.3	0
	>200	0.4 ± 0.3	0	1.4 ± 0.9	0	0.3 ± 0.2	0
>160	$50-100$	5.0 ± 1.5	3	13 ± 4	11	3.5 ± 1.1	2
	$100-150$	5.2 ± 1.4	7	9.0 ± 2.5	5	4.0 ± 1.2	6
	$150-200$	1.3 ± 0.5	2	3.4 ± 1.2	3	0.9 ± 0.3	0
	>200	1.6 ± 0.6	1	2.9 ± 0.9	5	1.3 ± 0.4	0

Table 11: Expected and observed yields in events with three e or μ that do not form an OSSF pair. Uncertainty denotes total uncertainty on the result.

M_{T} (GeV)	$E_{\mathrm{T}}^{\mathrm{miss}}$ (GeV)	$m_{\ell\ell} < 100$ GeV		$m_{\ell\ell} \geq 100$ GeV	
$0-120$	$50-100$	29 ± 7	26	2.6 ± 1.0	1
	>100	9.8 ± 2.6	12	0.8 ± 0.3	1
>120	>50	13 ± 3	11	3.0 ± 1.1	3

Table 12: Expected and observed yields in events with two e or μ forming and OSSF pair and one τ_{h}. Uncertainty denotes total uncertainty on the result.

$M_{\mathrm{T2}}(l,l)$ (GeV)	$E_{\mathrm{T}}^{\mathrm{miss}}$ (GeV)	$m_{\ell\ell} < 75$ GeV		$75 \leq m_{\ell\ell} < 105$ GeV		$m_{\ell\ell} \geq 105$ GeV	
<100	$50-100$	200 ± 50	162	1000 ± 300	1007	120 ± 33	114
	$100-150$	25 ± 7	27	38 ± 8	35	31 ± 9	20
	$150-200$	4.0 ± 1.5	2	11.3 ± 2.6	7	6.3 ± 2.2	7
	>200	3.3 ± 1.4	2	7.6 ± 1.8	7	4.3 ± 1.5	7

$M_{\mathrm{T2}}(l,l)$ (GeV)	$E_{\mathrm{T}}^{\mathrm{miss}}$ (GeV)	off-Z	
≥ 100	$50-200$	3.7 ± 1.1	6
	>200	0.5 ± 0.2	0

Table 13: Expected and observed yields in events with an opposite-sign eμ pair and one τ_{h}. Uncertainty denotes total uncertainty on the result.

$M_{\mathrm{T2}}(l,l)$ (GeV)	$E_{\mathrm{T}}^{\mathrm{miss}}$ (GeV)	$m_{\ell\ell} < 60$ GeV		$60 \leq m_{\ell\ell} < 100$ GeV		$m_{\ell\ell} \geq 100$ GeV	
<100	$50-100$	100 ± 30	82	97 ± 28	83	23 ± 7	25
	$100-150$	41 ± 12	27	32 ± 10	26	8.1 ± 2.7	7
	$150-200$	8.3 ± 2.5	10	8.5 ± 2.8	6	2.5 ± 1.1	4
	>200	4.8 ± 1.8	3	2.7 ± 1.1	6	1.4 ± 0.7	2
≥ 100	$50-200$	3.5 ± 1.4				1	
	>200	0.3 ± 0.3				0	

Table 14: Expected and observed yields in events with one same-sign e or μ and one τ_{h}. Uncertainty denotes total uncertainty on the result.

$M_{\mathrm{T2}}(l,\tau)$ (GeV)	$E_{\mathrm{T}}^{\mathrm{miss}}$ (GeV)	$m_{\ell\ell} < 60$ GeV		$60 \leq m_{\ell\ell} < 100$ GeV		$m_{\ell\ell} \geq 100$ GeV	
<100	$50-100$	19 ± 4	20	16 ± 4	26	1.6 ± 0.7	4
	$100-150$	4.5 ± 1.5	8	3.4 ± 1.0	5		
	$150-200$	1.4 ± 0.6	0	0.7 ± 0.3	1		
	>200	0.9 ± 0.3	0	0.5 ± 0.2	0		
≥ 100	>50	1.3 ± 0.5				1	

Table 15: Expected and observed yields in events with one e or μ and two τ_{h}. Uncertainty denotes total uncertainty on the result.

$M_{\mathrm{T2}}(l,\tau)$ (GeV)	$E_{\mathrm{T}}^{\mathrm{miss}}$ (GeV)	$m_{\ell\ell} < 100$ GeV		$m_{\ell\ell} \geq 100$ GeV	
<100	$50-100$	100 ± 28	82	30 ± 8	20
	$100-150$	16 ± 5	17	7.0 ± 2.1	6
	>150	6.5 ± 2.1	3	2.4 ± 0.9	2
≥ 100	$50-200$	2.9 ± 1.2		1	
	>200	0.5 ± 0.4		1	

Table 16: Expected and observed yields in the 4ℓ category of the analysis. The uncertainty denotes the total uncertainty on the result.

$E_{\mathrm{T}}^{\mathrm{miss}}$ (GeV)	$0\tau_h$				$\geq 1\tau_h$	
	nOSSF ≥ 2		nOSSF ≤ 1		nOSSF ≥ 0	
$0-30$	148 ± 40	193	3.1 ± 0.8	3	10.9 ± 2.6	19
$30-50$	50 ± 12	62	1.8 ± 0.4	0	7.8 ± 2.0	9
$50-100$	12.7 ± 2.9	11	2.7 ± 0.5	5	9.0 ± 2.3	6
>100	2.5 ± 0.5	2	3.5 ± 1.0	3	2.1 ± 0.7	2

Table 17: Search regions for events with two same-sign light flavor leptons. The uncertainties include both systematic and statistical components.

N_{jets}	M_{T} (GeV)	$p_{\mathrm{T}}^{\ell\ell}$ (GeV)	$E_{\mathrm{T}}^{\mathrm{miss}} < 100$ GeV		$100 \leq E_{\mathrm{T}}^{\mathrm{miss}} < 150$ GeV		$E_{\mathrm{T}}^{\mathrm{miss}} \geq 150$ GeV	
			exp	obs	exp	obs	exp	obs
0	<100	<50	310 ± 56	294	15 ± 4	16	1.8 ± 0.6	2
		≥ 50	180 ± 32	191	36 ± 8	33	7.9 ± 1.9	4
	≥ 100	-	32 ± 7	29	15 ± 3	9	15 ± 3	9
1	<100	<50	120 ± 25	127	33 ± 7	43	7.2 ± 1.5	14
		≥ 50	150 ± 29	146	49 ± 10	59	20 ± 4	39
	≥ 100	-	12 ± 2	13	8.7 ± 1.6	8	4.3 ± 1.0	6

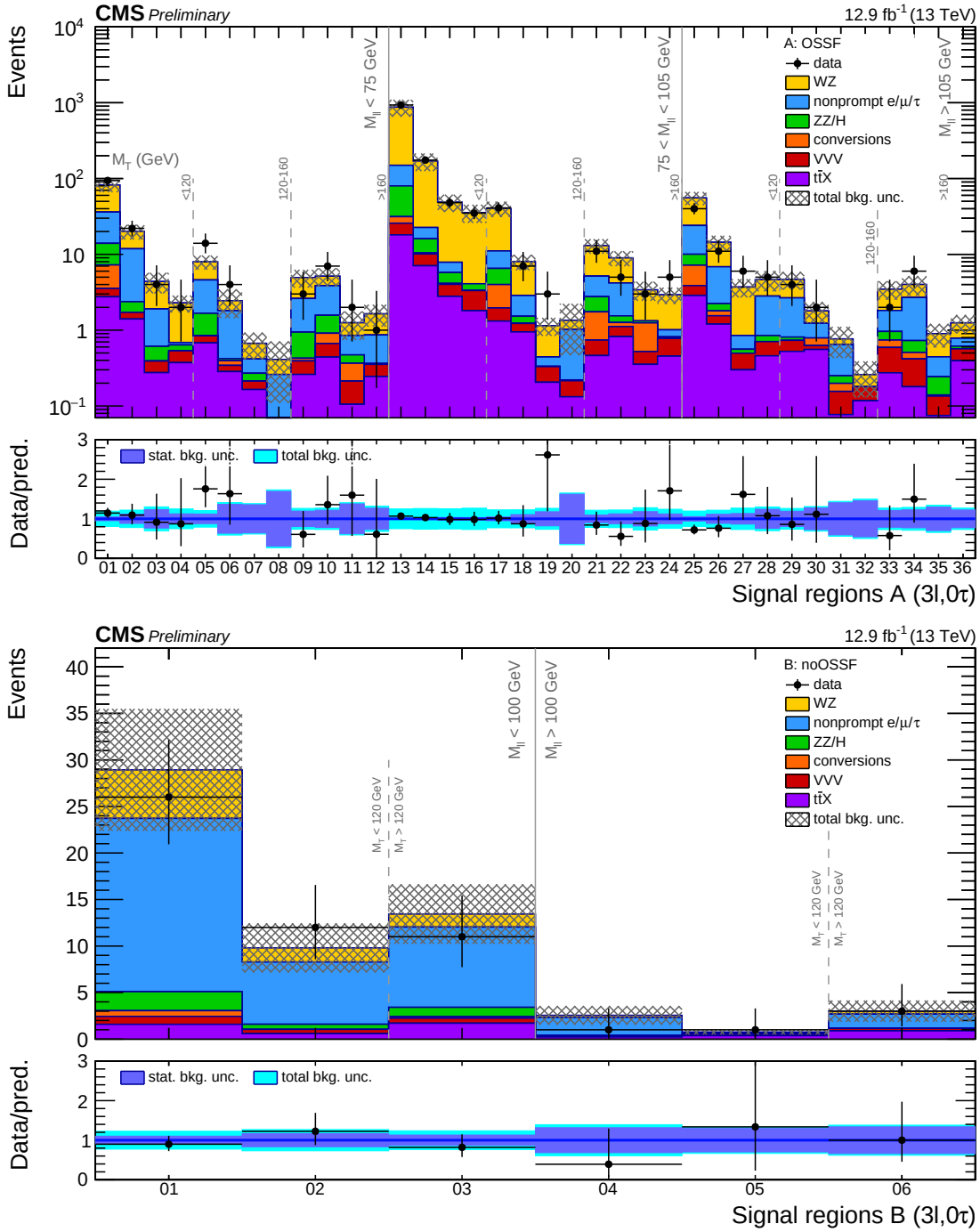

Figure 2: Comparison of the expected and observed yields in trilepton signal regions: three light leptons (top) with and (bottom) without an OSSF pair. The lower panel shows the ratio between the observed and expected yields in all signal regions, with the dark blue band indicating the statistical background uncertainty, and the light blue band corresponding to the total background uncertainty propagated to the ratio.

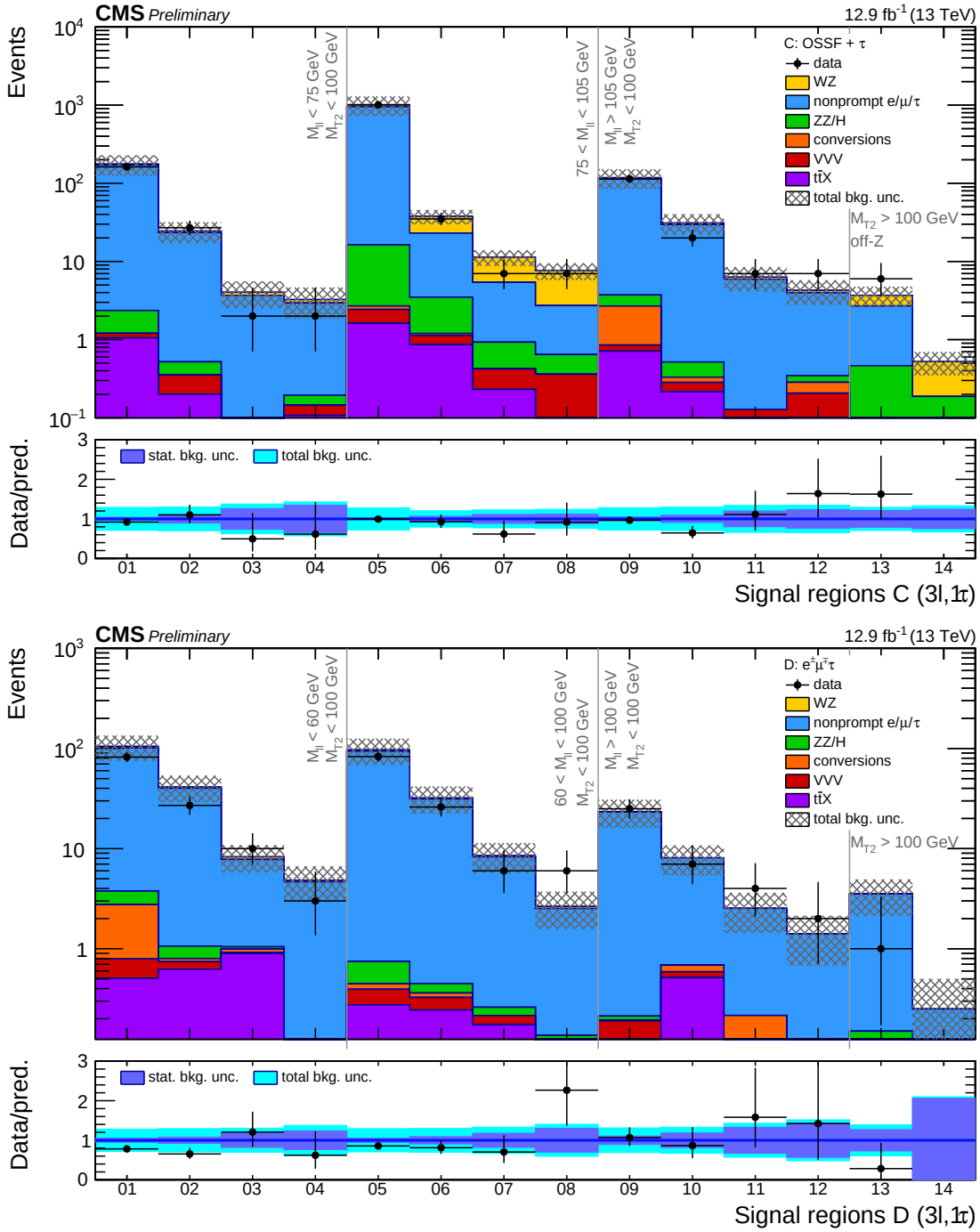

Figure 3: Comparison of the expected and observed yields in trilepton signal regions: τ_h and two light leptons of the opposite sign and same flavor (top) or different flavor (bottom). The lower panel shows the ratio between the observed and expected yields in all signal regions, with the dark blue band indicating the statistical background uncertainty, and the light blue band corresponding to the total background uncertainty propagated to the ratio.

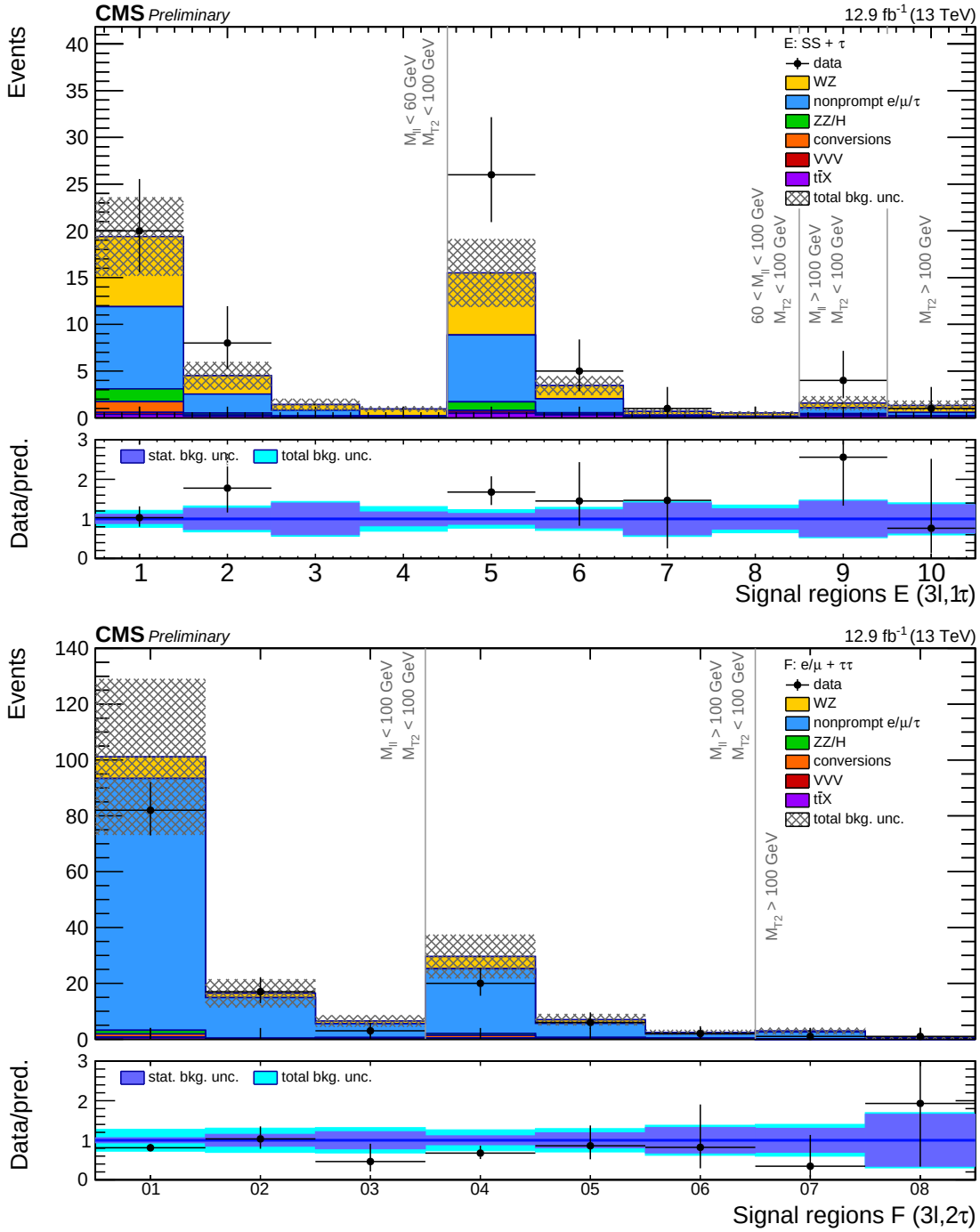

Figure 4: Comparison of the expected and observed yields in trilepton signal regions: two light leptons of the same sign and a τ_h (top), and a light lepton and two τ_h (bottom). The lower panel shows the ratio between the observed and expected yields in all signal regions, with the dark blue band indicating the statistical background uncertainty, and the light blue band corresponding to the total background uncertainty propagated to the ratio.

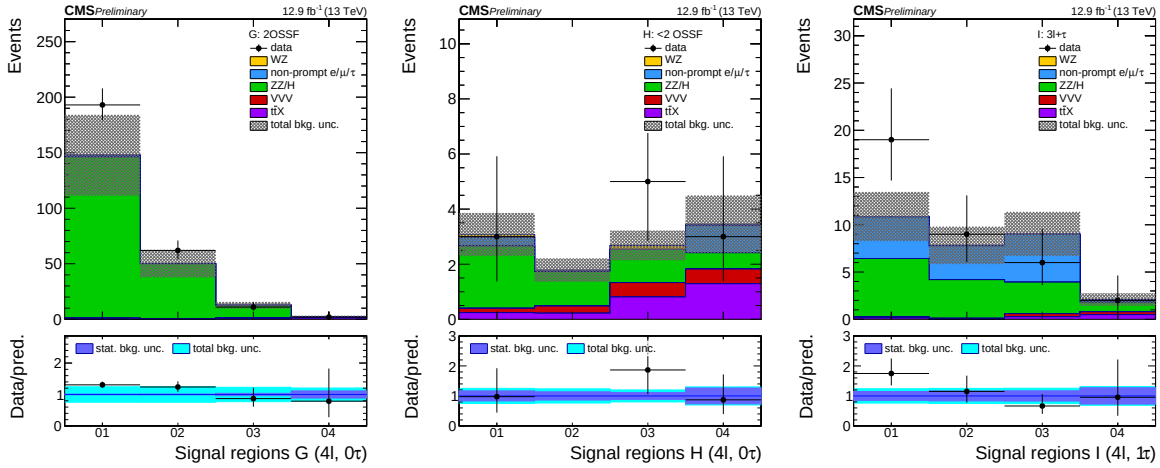

Figure 5: Comparison of the expected and observed yields in four lepton signal regions. The left plot shows the events with no taus and at least 2 OSSF pairs, the center plot shows events with no taus and less than 2 OSSF pairs while the right plot contains events with at least one τ_h. The lower panel shows the ratio between the observed and expected yields in all signal regions, with the dark blue band indicating the statistical background uncertainty, and the light blue band corresponding to the total background uncertainty propagated to the ratio.

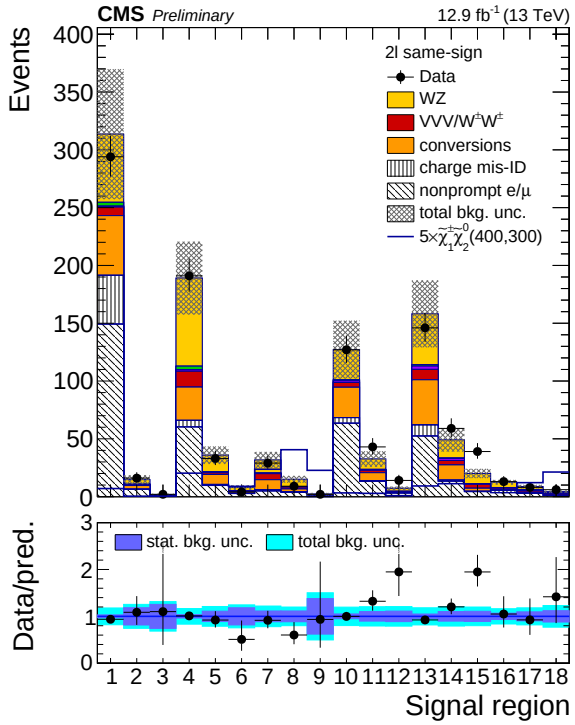

Figure 6: Expected yields and observed counts for the search regions defined in the same-sign dilepton category. The blue line represents the yield in the flavor-democratic scenario of $\widetilde{\chi}_2^0\widetilde{\chi}_1^\pm$ production with $m_{\widetilde{\chi}_2^0} = m_{\widetilde{\chi}_1^\pm} = 400\,\text{GeV}$, $m_{\widetilde{\chi}_1^0} = 300\,\text{GeV}$, and $x_{\tilde{\ell}} = 0.05$, scaled up by a factor of 5. The lower panel shows the ratio between the observed and expected yields in all signal regions, with the dark blue band indicating the statistical background uncertainty, and the light blue band corresponding to the total background uncertainty propagated to the ratio.

7 Interpretations of the searches

The results of the trilepton and same-sign dilepton searches are interpreted in the context of the simplified models of chargino-neutralino pair production. Four-lepton search regions, which are sensitive to the final states with two Z bosons and $E_{\mathrm{T}}^{\mathrm{miss}}$, are not used in the interpretations presented herein. We compute 95% confidence level (CL) upper limits on the new-physics cross sections using the $\mathrm{CL_s}$ method [46–48], incorporating the uncertainties on the signal efficiency and acceptance and the uncertainties on the expected background described in Section 5. The NLO+NLL cross sections from Refs. [49–51] are used to derive constraints on the masses of the charginos and neutralinos. The results from search regions with lepton flavor and charge requirements corresponding to the topology of the interpreted model are combined in order to increase sensitivity to the model in question.

Several scenarios of the mass hierarchy of gauginos and sleptons are considered in the interpretations as discussed in Section 1. In the case where sleptons and sneutrinos are lighter than $\widetilde{\chi}_2^0$ and $\widetilde{\chi}_1^{\pm}$, the sleptons are produced in the decay chains of the charginos and neutralinos as shown in Fig. 1a and 1b. The search sensitivity in these scenarios depends on the mass $m_{\tilde{\ell}}$ of the intermediate slepton (if left-handed, taken to be the same for its sneutrino $\widetilde{\nu}$), parametrized in terms of a variable $x_{\tilde{\ell}}$ as:

$$m_{\tilde{\ell}} = m_{\widetilde{\nu}} = m_{\widetilde{\chi}_1^0} + x_{\tilde{\ell}}\,(m_{\widetilde{\chi}} - m_{\widetilde{\chi}_1^0}), \tag{3}$$

where $0 < x_{\tilde{\ell}} < 1$. We consider interpretations for $x_{\tilde{\ell}} = 0.50$, i.e., the slepton mass equal to the mean of the LSP and the $\widetilde{\chi}$ masses, and in some cases for more compressed spectra with $x_{\tilde{\ell}} = 0.05$ or 0.95, i.e., the slepton mass close to either the LSP or the $\widetilde{\chi}$ mass, respectively.

The results for of the interpretation in the "flavor-democratic" scenario with $x_{\tilde{\ell}} = 0.5$ by using search regions from the trilepton search in category A are shown in Fig. 7. The corresponding interpretation for the mass hierarchy with $x_{\tilde{\ell}} = 0.05$ is summarized in Fig. 8. In this scenario, the same-sign dilepton search allows to probe the region where one of the leptons is out of the kinematical acceptance of the trilepton search. Figure 8a shows the interpretation obtained with the search regions from the category A of the trilepton search, Fig. 8b contains the results obtained with the same-sign dilepton search regions, and Fig. 8c shows the combination of the two searches.

Figure 9 shows the results of the interpretation of the trilepton search in the tau-dominated scenario. In this case search regions B, D, E and F are used to place limits on the production cross section of charginos and neutralinos.

If the sleptons are too heavy and do not enter the cascade decays of the gauginos, we consider a scenario where a chargino is assumed to always decay to a W boson and the $\widetilde{\chi}_1^0$ LSP, while a neutralino can decay to a Z boson or the Higgs boson and an LSP. We consider two limiting cases, in which either $\mathcal{B}(\widetilde{\chi}_2^0 \to \mathrm{Z}\widetilde{\chi}_1^0) = 1$, or $\mathcal{B}(\widetilde{\chi}_2^0 \to \mathrm{H}\widetilde{\chi}_1^0) = 1$. The sensitivity in a generic model lies between these two extremes. Figure 10a shows the interpretation for the final state with a W and Z boson pair and $E_{\mathrm{T}}^{\mathrm{miss}}$ obtained with the results of the trilepton search in category A events. In Figure 10b the interpretation for final states with a W and H boson pair and $E_{\mathrm{T}}^{\mathrm{miss}}$ is shown, which is a result of the combination of all 88 trilepton search regions A-F.

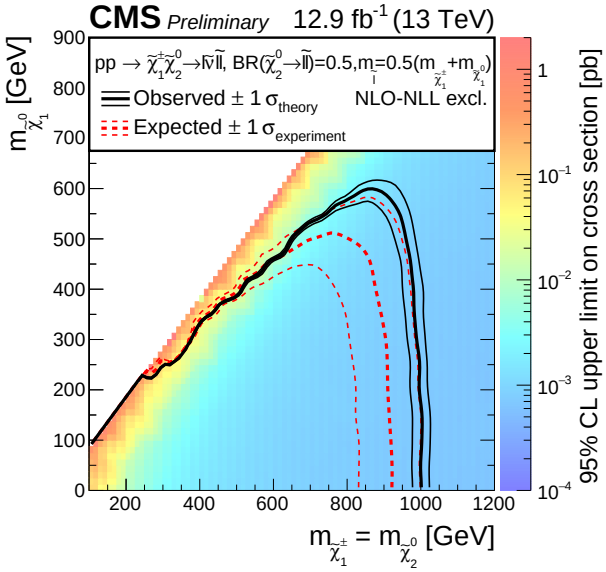

Figure 7: Interpretation of the results of the three-lepton search in the flavor-democratic signal model with slepton mass parameter $x_{\tilde{\ell}} = 0.5$. The shading in the $m_{\tilde{\chi}_1^0}$ versus $m_{\tilde{\chi}_2^0}$ $(= m_{\tilde{\chi}_1^\pm})$ plane indicates the 95% CL upper limit on the chargino-neutralino production cross section times branching fraction. The contours bound the mass regions excluded at 95% CL assuming the NLO+NLL cross sections for a branching fraction of 50%, as appropriate for the visible decay products in this scenario. The observed, $\pm 1\sigma_{\text{theory}}$ observed, median expected, and $\pm 1\sigma_{\text{experiment}}$ expected bounds are shown.

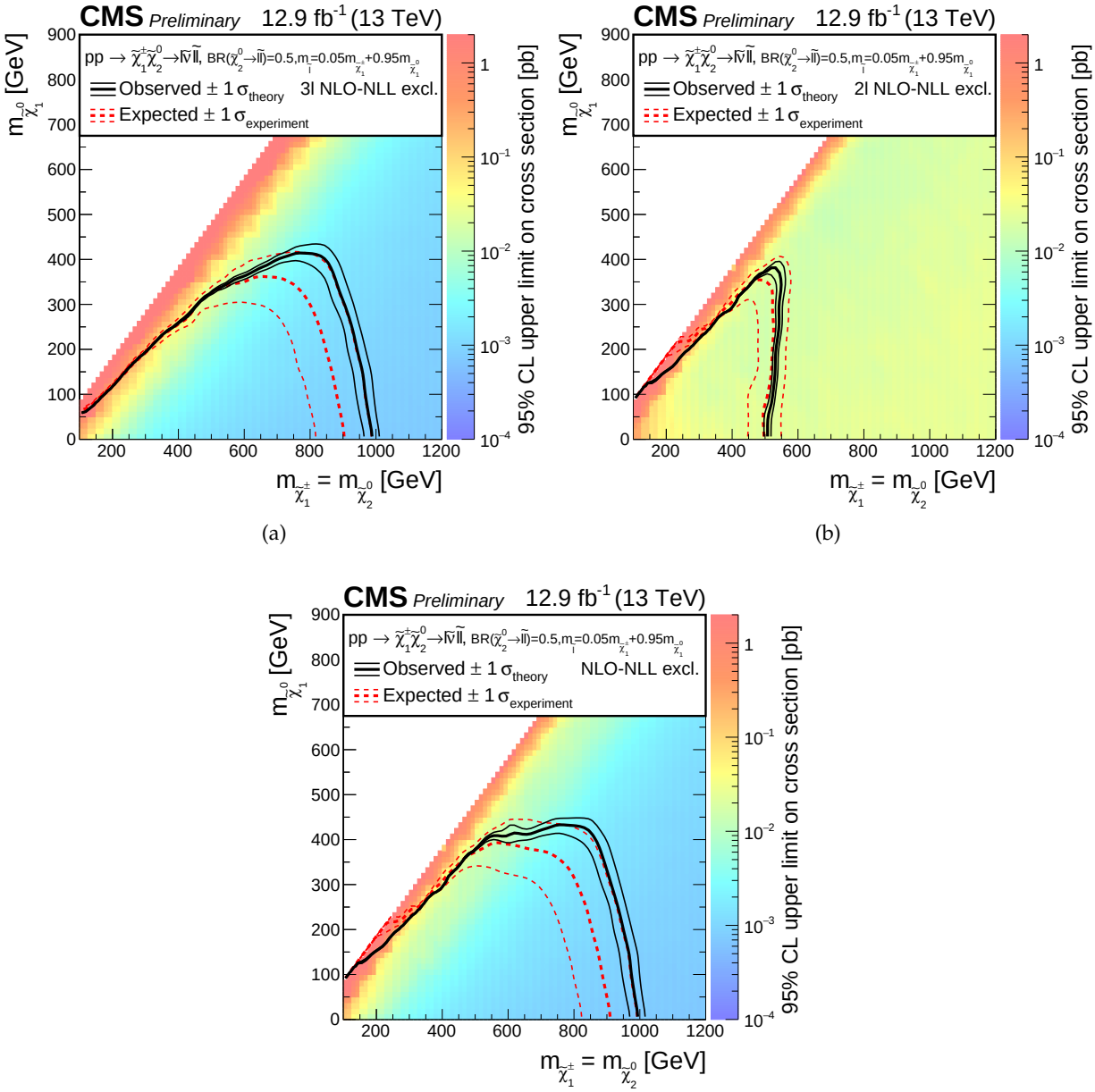

Figure 8: Interpretation of the results of the three-lepton search in the flavor-democratic signal model with slepton mass parameter $x_{\tilde{\ell}} = 0.05$ obtained with (a) trilepton search, (b) same-sign dilepton search and (c) the combination of the two analyses. The shading in the $m_{\widetilde{\chi}_1^0}$ versus $m_{\widetilde{\chi}_2^0}$ ($= m_{\widetilde{\chi}_1^\pm}$) plane indicates the 95% CL upper limit on the chargino-neutralino production cross section times branching fraction. The contours bound the mass regions excluded at 95% CL assuming the NLO+NLL cross sections for a branching fraction of 50%, as appropriate for the visible decay products in this scenario. The observed, $\pm 1\sigma_{\text{theory}}$ observed, median expected, and $\pm 1\sigma_{\text{experiment}}$ expected bounds are shown.

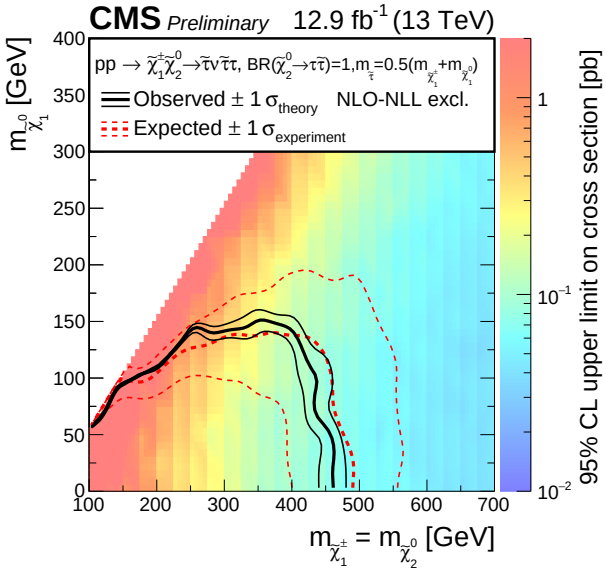

Figure 9: Interpretation of the results of the three-lepton search in the tau-dominated signal model with slepton mass parameter $x_{\tilde{\ell}} = 0.5$. The shading in the $m_{\tilde{\chi}_1^0}$ versus $m_{\tilde{\chi}_2^0}$ $(= m_{\tilde{\chi}_1^\pm})$ plane indicates the 95% CL upper limit on the chargino-neutralino production cross section times branching fraction. The contours bound the mass regions excluded at 95% CL assuming the NLO+NLL cross sections for a branching fraction of 100%. The observed, $\pm 1\sigma_{\text{theory}}$ observed, median expected, and $\pm 1\sigma_{\text{experiment}}$ expected bounds are shown.

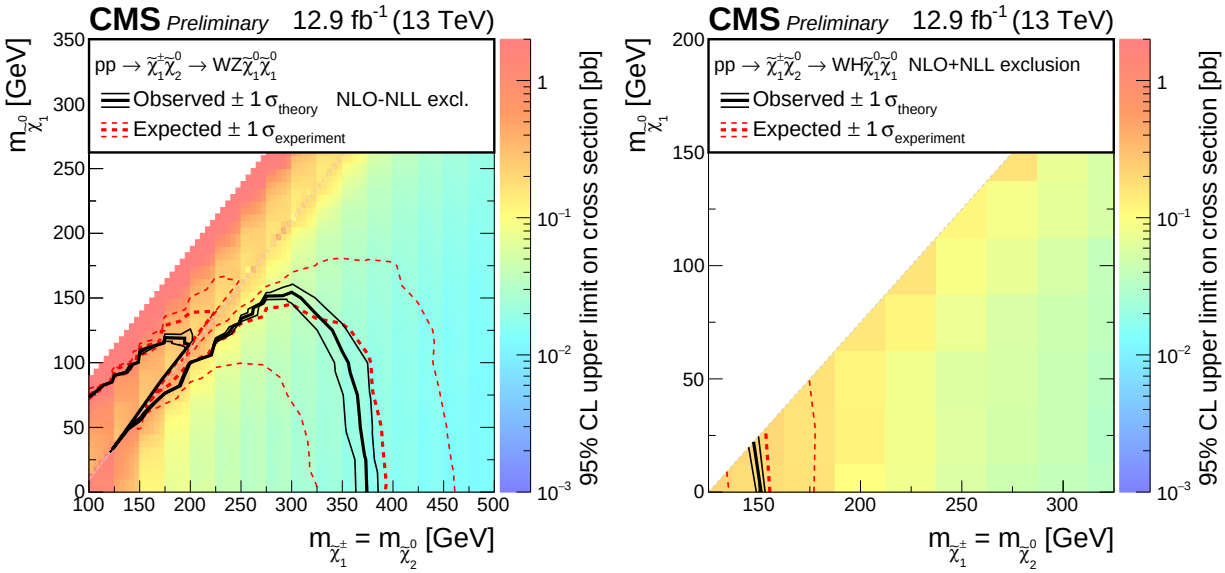

(a) WZ scenario (b) WH scenario

Figure 10: Interpretation of the results of the three-lepton search in the scenarios without intermediate light sleptons present and yielding (a) WZ+$E_{\text{T}}^{\text{miss}}$ or (b) WH+$E_{\text{T}}^{\text{miss}}$ in the final state. The shading in the $m_{\tilde{\chi}_1^0}$ versus $m_{\tilde{\chi}_2^0}$ $(= m_{\tilde{\chi}_1^\pm})$ plane indicates the 95% CL upper limit on the chargino-neutralino production cross section times branching fraction. The contours bound the mass regions excluded at 95% CL assuming the NLO+NLL cross sections for a branching fraction of 100%. The observed, $\pm 1\sigma_{\text{theory}}$ observed, median expected, and $\pm 1\sigma_{\text{experiment}}$ expected bounds are shown.

8 Summary

The results of a search for new physics in same-sign dilepton, trilepton and four-lepton events containing up to two hadronically decaying τ_h using the CMS detector at the LHC and based on a data sample of pp collisions at $\sqrt{s} = 13\,\text{TeV}$, corresponding to an integrated luminosity of 12.9 fb^{-1}, are presented. The data are split into categories formed according to the number, sign and flavor of the leptons, and are further subdivided in various kinematic regions to be sensitive to a broad range of electroweakly produced new particles.

No significant deviation from the standard model expectations is observed. The results are used to set limits on the various simplified models with a chargino-neutralino pair production which is the electroweak SUSY process with the largest cross section. The resulting signal topologies depend on the masses of the sleptons. Models with light left sleptons enhance the branching fraction to final states with three leptons. Depending on the left/right mixing and flavor of these sleptons, our results probe charginos and neutralinos with masses up to 1 TeV for the flavor-democratic scenario which extends the reach of the previous result [11] by about 300 GeV. In these models, searches in the same-sign dilepton final state enhance the sensitivity in the experimentally challenging region with small mass difference between the produced gauginos and an LSP, and allow to probe the regions inaccessible by the trilepton signature.

In case chargino and neutralino decay to three taus and LSP in the final state, the masses of charginos up to 450 GeV are probed, extending the sensitivity of the previous search by 150 GeV.

The most challenging considered scenarios are the direct decay of produced gauginos to LSP via W and Z or Higgs bosons. For the final states with W and Z bosons, the chargino masses is probed up to 400 GeV. This improves the previous reach by 130 GeV. In case of the neutralino decay via a Higgs boson, only masses up to 150 GeV can be probed, which does not add a new sensitivity over results achieved in the previous searches.

References

[1] P. Ramond, "Dual theory for free fermions", *Phys. Rev. D* **3** (1971) 2415, doi:10.1103/PhysRevD.3.2415.

[2] Yu. A. Golfand and E. P. Likhtman, "Extension of the algebra of Poincare group generators and violation of P invariance", *JETP Lett.* **13** (1971) 323. [Pisma Zh. Eksp. Teor. Fiz. 13 (1971) 452].

[3] A. Neveu and J. H. Schwarz, "Factorizable dual model of pions", *Nucl. Phys. B* **31** (1971) 86, doi:10.1016/0550-3213(71)90448-2.

[4] D. V. Volkov and V. P. Akulov, "Possible universal neutrino interaction", *JETP Lett.* **16** (1972) 438. [Pisma Zh. Eksp. Teor. Fiz. 16 (1972) 621].

[5] J. Wess and B. Zumino, "A lagrangian model invariant under supergauge transformations", *Phys. Lett. B* **49** (1974) 52, doi:10.1016/0370-2693(74)90578-4.

[6] J. Wess and B. Zumino, "Supergauge transformations in four-dimensions", *Nucl. Phys. B* **70** (1974) 39, doi:10.1016/0550-3213(74)90355-1.

[7] P. Fayet, "Supergauge invariant extension of the Higgs mechanism and a model for the electron and its neutrino", *Nucl. Phys. B* **90** (1975) 104, doi:10.1016/0550-3213(75)90636-7.

[8] H. P. Nilles, "Supersymmetry, supergravity and particle physics", *Phys. Rept.* **110** (1984) 1, doi:10.1016/0370-1573(84)90008-5.

[9] S. P. Martin, "A supersymmetry primer", in *Perspectives on Supersymmetry II*, G. L. Kane, ed., p. 1. 2010. arXiv:hep-ph/9709356. Adv. Ser. Direct. High Energy Phys., vol. 21. doi:10.1142/9789814307505_0001.

[10] CMS Collaboration, "Phenomenological MSSM interpretation of CMS searches in pp collisions at $\sqrt{s}$ = 7 and 8 TeV", arXiv:1606.03577.

[11] CMS Collaboration, "Searches for electroweak production of charginos, neutralinos, and sleptons decaying to leptons and W, Z, and Higgs bosons in pp collisions at 8 TeV", *Eur. Phys. J. C* **74** (2014), no. 9, 3036, doi:10.1140/epjc/s10052-014-3036-7, arXiv:1405.7570.

[12] CMS Collaboration, "Searches for electroweak neutralino and chargino production in channels with Higgs, Z, and W bosons in pp collisions at 8 TeV", *Phys. Rev. D* **90** (2014), no. 9, 092007, doi:10.1103/PhysRevD.90.092007, arXiv:1409.3168.

[13] CMS Collaboration, "Search for supersymmetry in the multijet and missing transverse momentum final state in pp collisions at 13 TeV", *Phys. Lett. B* **758** (2016) 152–180, doi:10.1016/j.physletb.2016.05.002, arXiv:1602.06581.

[14] CMS Collaboration, "Search for new physics with the MT2 variable in all-jets final states produced in pp collisions at $\sqrt{s}$ = 13 TeV", arXiv:1603.04053.

[15] CMS Collaboration, "Search for supersymmetry in pp collisions at $\sqrt{s}$ = 13 TeV in the single-lepton final state using the sum of masses of large-radius jets", arXiv:1605.04608.

[16] CMS Collaboration, "Search for new physics in same-sign dilepton events in proton-proton collisions at $\sqrt{s}$ = 13 TeV", arXiv:1605.03171.

[17] CMS Collaboration, "The CMS experiment at the CERN LHC", *JINST* **3** (2008) S08004, doi:10.1088/1748-0221/3/08/S08004.

[18] CMS Collaboration, "Particle-Flow Event Reconstruction in CMS and Performance for Jets, Taus, and MET", CMS Physics Analysis Summary CMS-PAS-PFT-09-001, 2009.

[19] CMS Collaboration, "Commissioning of the Particle–Flow reconstruction in Minimum–Bias and Jet Events from pp Collisions at 7 TeV", CMS Physics Analysis Summary CMS-PAS-PFT-10-002, 2010.

[20] M. Cacciari, G. P. Salam, and G. Soyez, "FastJet User Manual", *Eur. Phys. J. C* **72** (2012) 1896, doi:10.1140/epjc/s10052-012-1896-2, arXiv:1111.6097.

[21] M. Cacciari and G. P. Salam, "Dispelling the N^3 myth for the k_T jet-finder", *Phys. Lett. B* **641** (2006) 57–61, doi:10.1016/j.physletb.2006.08.037, arXiv:hep-ph/0512210.

[22] CMS Collaboration, "Determination of jet energy calibration and transverse momentum resolution in CMS", *JINST* **6** (2011) P11002, doi:10.1088/1748-0221/6/11/P11002, arXiv:1107.4277.

[23] CMS Collaboration, "Identification of b quark jets at the CMS Experiment in the LHC Run 2", CMS Physics Analysis Summary CMS-PAS-BTV-15-001, CERN, 2016.

[24] CMS Collaboration, "Performance of the CMS missing transverse momentum reconstruction in pp data at $\sqrt{s} = 8$ TeV", *JINST* **10** (2015) P02006, doi:10.1088/1748-0221/10/02/P02006, arXiv:1411.0511.

[25] CMS Collaboration, "Performance of CMS muon reconstruction in pp collision events at $\sqrt{s} = 7$ TeV", *JINST* **7** (2012) P10002, doi:10.1088/1748-0221/7/10/P10002, arXiv:1206.4071.

[26] CMS Collaboration, "Performance of electron reconstruction and selection with the CMS detector in proton-proton collisions at $\sqrt{s} = 8$ TeV", *JINST* **10** (2015) P06005, doi:10.1088/1748-0221/10/06/P06005, arXiv:1502.02701.

[27] K. Rehermann and B. Tweedie, "Efficient identification of boosted semileptonic top quarks at the LHC", *JHEP* **03** (2011) 059, doi:10.1007/JHEP03(2011)059, arXiv:1007.2221.

[28] CMS Collaboration, "Search for $\mathrm{t\bar{t}H}$ production in multilepton final states at $\sqrt{s}$ = 13 TeV", CMS Physics Analysis Summary CMS-PAS-HIG-15-008, 2016.

[29] B. P. Roe et al., "Boosted decision trees, an alternative to artificial neural networks", *Nucl. Instrum. Meth. A* **543** (2005), no. 2-3, 577–584, doi:10.1016/j.nima.2004.12.018, arXiv:physics/0408124.

[30] CMS Collaboration, "Reconstruction and identification of τ lepton decays to hadrons and ν_τ at CMS", *JINST* **11** (2016), no. 01, P01019, doi:10.1088/1748-0221/11/01/P01019, arXiv:1510.07488.

[31] CMS Collaboration, "Performance of reconstruction and identification of tau leptons in their decays to hadrons and tau neutrino in LHC Run-2", CMS Physics Analysis Summary CMS-PAS-TAU-16-002, 2016.

[32] J. Alwall et al., "The automated computation of tree-level and next-to-leading order differential cross sections, and their matching to parton shower simulations", *JHEP* **07** (2014) 079, doi:10.1007/JHEP07(2014)079, arXiv:1405.0301.

[33] T. Melia, P. Nason, R. Rontsch, and G. Zanderighi, "W^+W^-, WZ and ZZ production in the POWHEG BOX", *JHEP* **11** (2011) 078, doi:10.1007/JHEP11(2011)078, arXiv:1107.5051.

[34] P. Nason and G. Zanderighi, "W^+W^-, WZ and ZZ production in the POWHEG-BOX-V2", *Eur. Phys. J. C* **74** (2014) 2702, doi:10.1140/epjc/s10052-013-2702-5, arXiv:1311.1365.

[35] NNPDF Collaboration, "Parton distributions for the LHC Run II", *JHEP* **04** (2015) 040, doi:10.1007/JHEP04(2015)040, arXiv:1410.8849.

[36] T. Sjöstrand, S. Mrenna, and P. Z. Skands, "A brief introduction to PYTHIA 8.1", *Comput. Phys. Commun.* **178** (2008) 852, doi:10.1016/j.cpc.2008.01.036, arXiv:0710.3820.

[37] P. Skands, S. Carrazza, and J. Rojo, "Tuning PYTHIA 8.1: the Monash 2013 tune", *Eur. Phys. J. C* **74** (2014) 3024, doi:10.1140/epjc/s10052-014-3024-y, arXiv:1404.5630.

[38] CMS Collaboration, "Event generator tunes obtained from underlying event and multiparton scattering measurements", *Eur. Phys. J. C* **76** (2016) 155, doi:10.1140/epjc/s10052-016-3988-x, arXiv:1512.00815.

[39] GEANT4 Collaboration, "GEANT4—a simulation toolkit", *Nucl. Instrum. Meth. A* **506** (2003) 250, doi:10.1016/S0168-9002(03)01368-8.

[40] S. Abdullin et al., "The fast simulation of the CMS detector at LHC", *J. Phys. Conf. Ser.* **331** (2011) 032049, doi:10.1088/1742-6596/331/3/032049.

[41] D. Alves et al., "Simplified models for LHC new physics searches", *J. Phys. G* **39** (2012) 105005, doi:10.1088/0954-3899/39/10/105005, arXiv:1105.2838.

[42] CMS Collaboration, "Interpretation of searches for supersymmetry with simplified models", *Phys. Rev. D* **88** (2013) 052017, doi:10.1103/PhysRevD.88.052017, arXiv:1301.2175.

[43] C. G. Lester and D. J. Summers, "Measuring masses of semiinvisibly decaying particles pair produced at hadron colliders", *Phys. Lett. B* **463** (1999) 99, doi:10.1016/S0370-2693(99)00945-4, arXiv:hep-ph/9906349.

[44] A. Barr, C. Lester, and P. Stephens, "m(T2): The truth behind the glamour", *J. Phys. G* **29** (2003) 2343, doi:10.1088/0954-3899/29/10/304, arXiv:hep-ph/0304226.

[45] CMS Collaboration, "CMS luminosity measurement for the 2015 data taking period", CMS Physics Analysis Summary CMS-PAS-LUM-15-001, CERN, 2016.

[46] T. Junk, "Confidence level computation for combining searches with small statistics", *Nucl. Instrum. Meth. A* **434** (1999) 435, doi:10.1016/S0168-9002(99)00498-2, arXiv:hep-ex/9902006.

[47] A. L. Read, "Presentation of search results: The CL_s technique", *J. Phys. G* **28** (2002) 2693, doi:10.1088/0954-3899/28/10/313.

[48] ATLAS and CMS Collaborations, "Procedure for the LHC Higgs boson search combination in summer 2011", Technical Report ATL-PHYS-PUB-2011-11, CMS-NOTE-2011-005, 2011.

[49] B. Fuks, M. Klasen, D. R. Lamprea, and M. Rothering, "Gaugino production in proton-proton collisions at a center-of-mass energy of 8 TeV", *JHEP* **10** (2012) 081, doi:10.1007/JHEP10(2012)081, arXiv:1207.2159.

[50] B. Fuks, M. Klasen, D. R. Lamprea, and M. Rothering, "Precision predictions for electroweak superpartner production at hadron colliders with RESUMMINO", *Eur. Phys. J. C* **73** (2013) 2480, doi:10.1140/epjc/s10052-013-2480-0, arXiv:1304.0790.

[51] B. Fuks, M. Klasen, D. R. Lamprea, and M. Rothering, "Revisiting slepton pair production at the Large Hadron Collider", *JHEP* **01** (2014) 168, doi:10.1007/JHEP01(2014)168, arXiv:1310.2621.